BPR MCS Bulletin of Pioneering Researches of Medical and Clinical Science

Bulletin of Pioneering Researches of Medical and Clinical Science

Available online: https://bprmcs.com
2024 | Volume 4 | Issue 1 | Page: 186-200

Data-Driven Estimation of Rowing Forces and Power via Long Short-Term Memory Neural Networks

Lucas Meyer[1]*, Anna Schmid[2], Stefan Braun[1]

[1]Department of Medical Research Systems, ETH Zurich, Zurich, Switzerland.
[2]Department of Clinical Investigation Sciences, University of Bern, Bern, Switzerland.

Abstract

Assessing rowing output, such as by examining force and power delivery curves from an ergometer or a boat, is a top priority for coaches and athletes alike. The gold-standard approaches currently available for rowing output evaluation require purpose-built sensorized hardware, with PowerLine and BioRow being the most widely adopted options. This workflow is both financially demanding and labor-intensive, thereby reducing the frequency with which coaches can oversee rowers. In this work, we devised a simpler-to-mount, lower-cost technique for inferring rowers' forces and powers using only cable-position transducers for indoor rowing and inertial measurement units (IMUs) and GPS for on-water sculling. Recordings from 12 and 11 rowers, on an ergometer and in a boat, respectively, were used to learn the parameters of a long short-term memory (LSTM) network. The LSTM proved capable of recovering gate forces and power, with a total mean absolute error remaining below 5%. The recovered force and power profiles uncovered technical differences between individuals, attaining 93% accuracy. Undertaking leave-one-out cross-validation resulted in a substantial increase in error, supporting the conclusion that a broader pool of participants is necessary to yield a model that generalizes to unseen rowers.

Keywords: Machine learning, Rowing, IMU, Kinetics, LSTM

Corresponding author: Lucas Meyer
E-mail: lucas.meyer@gmail.com

How to Cite This Article: Meyer L, Schmid A, Braun S. Data-Driven Estimation of Rowing Forces and Power via Long Short-Term Memory Neural Networks. Bull Pioneer Res Med Clin Sci. 2024;4(1):186-200. https://doi.org/10.51847/GJR2UDTUZl

Introduction

The sport of rowing demands meticulous synchronization across all body parts, which positions technique as a performance-defining element—one where race decisions can rest on gaps of merely a fraction of a second [1, 2]. Rowing features rhythmic, recurring motions, each cycle conventionally split into the drive and the recovery. The drive portion initiates upon blade entry, a juncture termed the 'catch.' Through the drive, the blades stay submerged, advancing the hull [1]. Within this portion, the successive engagement of legs, trunk, and arms yields power that is ultimately dispatched to the fluid via the oars [1]. The motion terminates as the blades exit the water—the 'finish' event—which commences the recovery portion. In recovery, the blades are airborne, and rowers use their feet to tug the hull back beneath them to prime for the upcoming cycle. When outdoor weather prohibits water sessions, rowers commonly resort to indoor rowing machines [3]. Select ergometer designs seek to mirror boat forces and motions as authentically as possible, featuring a free-floating assembly that lets the main frame translate horizontally [3].

Substantial recent work has focused on accurately recording and parameterizing rowing technique (often

labeled the "athlete signature" [4]) and its output via motion and force sensors embedded in shells and indoor trainers [4-12]. Force and power tracings attract special scrutiny because they relate to competitive success [1, 13] and to vertebral stresses associated with low back pain, a frequent complaint in rowing communities [14, 15]. Scrutiny of force–time graphs also serves as a selection criterion when forming crews for pair and quad boats [1, 16]. Moreover, resolving total rower-generated power into the partial contributions of separate body segments (i.e., arms, trunk, and legs) offers a compelling tool for defining an athlete's style and, in turn, spotting and adjusting technical shortcomings [1, 17, 18]. To numerically capture such force and power tracings, relevant metrics include time to peak (T2P), mean-to-peak ratio (M2P), and work ratio (WR). Flatter force profiles, reflected in a larger M2P [12, 13], and an earlier maximum in force conveyed to the oars (i.e., a smaller T2P) [9, 12] have both been correlated to higher achievement. Likewise, an earlier maxima of trunk power has been tied to superior achievement [17], a variable that may be specifically addressed via live biofeedback to refine a sculler's technical patterns [18].

Although recording the forces generated by athletes furnishes trainers with meaningful insights, it requires exchanging selected boat or machine parts for specialized, sensor-laden substitutes. Two of the most commonplace solutions for rowing output diagnostics are BioRow (BioRow Tech, London, UK) and PowerLine (Peach Innovation, Cambridge, UK). The arrangements put forward **(Figure 1)** involve swapping the foot stretcher (the fixture coupling to the rower's feet, enabling push–pull force transmission) in on-water and indoor scenarios, exchanging the oarlocks positioned at the boat gates (hull structures that restrain the oars, permitting them to swivel across the stroke arc), and attaching a strain gauge to the handle during stationary ergometer use (on an ergometer, oars are replaced by a solitary rigid handle linked to a chain) [4, 5, 8, 12, 19]. This kind of hardware can be pricey, and significant effort is required to maintain consistent rigging settings after component changes, most critically in sculling, where shells are meticulously adjusted to each individual's anthropometry and preferences [1]. These obstacles unavoidably cap the number of shells or machines that can be outfitted in parallel and the rate at which the sensorized pieces can be shifted between hulls, thereby curtailing the individualized observation a coach can allocate to each athlete. A procedure that infers rower-generated forces and powers without requiring any swapping of boat or ergometer components would be immensely useful, enabling quick instrumentation and monitoring of many rowers within a single club.

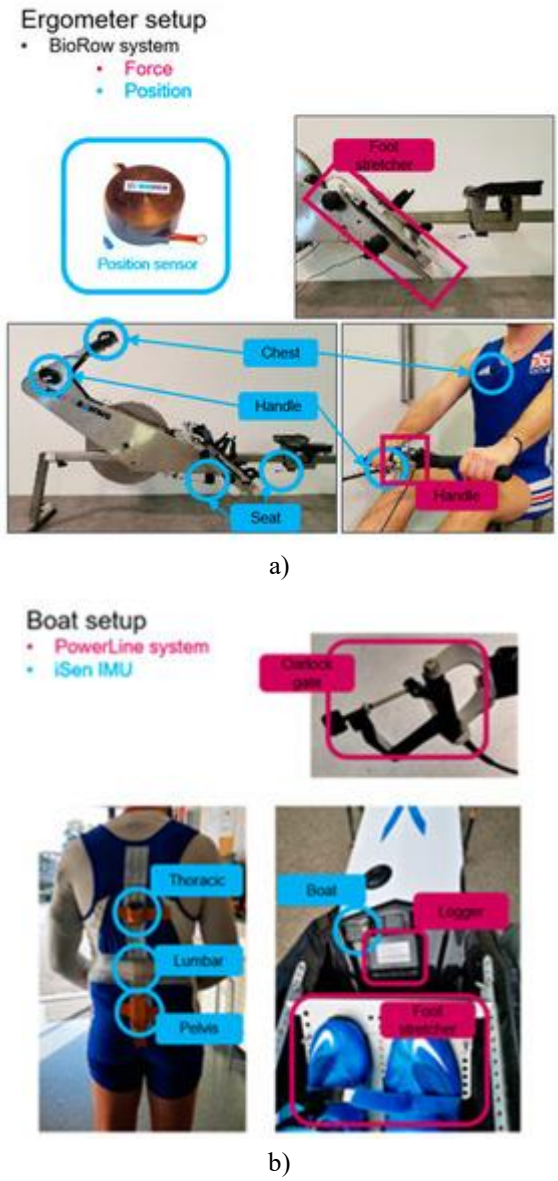

Figure 1. Sensor setup for ergometer and boat rowing.

Machine learning strategies have seen expansive deployment for recognizing human activity, most prominently within the biomechanics arena. These applications cover the sorting and identification of specific movement signatures, such as gait deviations [20, 21] and stroke mechanics in swimming [22], as well as the prediction of joint centers [23], skeletal configurations [24], and forces exchanged with the ground [25]. More recently, enterprises have begun crafting machine learning pipelines grounded in physics-informed biomechanical modeling to estimate internal tissue and surface contact loads from video streams [26, 27]. Within the rowing domain specifically, machine learning has been used to group rowers based on kinematic patterns [28], to distinguish novices from experts using posture recorded by inertial measurement units (IMUs) [29], and to slot rowers into particular competition classes informed by kinematics and demographic information [30].

An alternative to machine learning is the application of conventional biomechanical simulations. Predictive and tracking simulations, in particular, have been effectively utilized to explore human movement [31-33] and are highly appropriate for deducing forces and power output in the context of rowing. Tracking simulations perform forward dynamics while compelling the motion to adhere closely to the captured kinematics, allowing the reconstruction of dynamically coherent kinematics and kinetics even without directly recorded forces [31]. Nonetheless, this strategy is hindered by its greater computational load and the need for specialized users to manage the multiple facets of the simulation, including the formulation of models that depict muscle architecture, force production, and interactions with the environment.

To the best of our awareness, no machine learning approaches currently exist for deducing the forces and power delivered by rowers, with post-session interpretation of PowerLine or BioRow measurements remaining the benchmark for rowing output assessment. This article adds to established knowledge by providing a method for inferring rowing forces and powers from recorded kinematics.

Our principal aim was to reconstruct the time-varying waveforms of force and power throughout the rowing cycle rather than grouping athletes by technical style [28] or applying classifiers to rate their proficiency [29]. Because rowing is sequential by nature, exhibiting time-dependent force fluctuations and a progressive, ordered engagement of body parts, we opted to construct this work upon a recurrent neural network. Long short-term memory (LSTM) architectures are uniquely designed for processing sequential data and have seen extensive deployment in sequence-to-sequence tasks spanning many fields for years [34], including biomechanics, for recognizing motor patterns [34], anticipating falls [35], gait kinematics [36, 37], and gait cycle subdivisions [36]. The internal mechanics of LSTM networks have been covered in meticulous detail across numerous sources [37-40] and fall outside the remit of this paper. Briefly, the structural design of LSTM networks enables them to encode long-term temporal dependencies within sequences and to deliberately preserve or discard information [40].

The inputs fed into our proposed model needed to be sourced from inexpensive, non-intrusive sensors. For ergometer-based rowing, cable-driven position transducers can be utilized to track the displacements of various body segments [17, 18]. These devices employ a spring-tensioned cable that affixes and detaches easily to a rower's attire or the ergometer seat. Out on the water, the most adaptable solution for capturing rower motion is IMUs. IMUs constitute miniature, low-mass sensors that rowers can wear without discomfort or any motion restriction and that attach to the hull without altering the existing rigging. Given their flexibility, IMUs have found widespread use in quantifying human movement [32, 41-43].

The intention behind this study was to train an LSTM network to predict the forces and powers rowers produce during on-water and ergometer rowing, completely sidestepping the use of force transducers. More precisely, we set out to compute the forces acting at the feet and gates or handle, the power fed into the gates or handle, and the powers separately contributed by the arms, trunk, and legs. We hypothesize that the fidelity of force and power reconstruction would be sufficient to characterize each rower's technical signature, as captured by markers such as the location of the peak and the development ratio.

Materials and Methods

Participants

Data underpinning this investigation came from earlier published projects [12, 18]. The pool comprised 12 male scull-boat rowers (20.0 ± 2 years of age, 185 ± 5 cm, 79.0 ± 6.7 kg) and 11 male ergometer rowers (22.3 ± 2.2 years, 185.5 ± 7.1 cm, 77.4 ± 7.0 kg). No participant was contending with a recent injury.

Test procedure

For the on-water dataset, rowers were directed to row at the stroke rate they use in competition, which averaged 32.5 strokes per min (spm), and to use their own scull boats. The ergometer dataset included rowing trials at two stroke rates: 20 spm and the athlete's competition rate, averaging 35.8 spm.

Setup and data acquisition

The ergometer (RP3®, Care RowPerfect BV, Hardenberg, The Netherlands) was configured with BioRow sensing equipment. This included force-measuring units at the feet and handle and displacement-measuring units at the handle, seat, and chest **(Figure 1)**. The position-measuring devices relied on spring-retracting cables. These sensing units were coupled to a data acquisition board (National Instruments, "NI USB-6000 Multifunction I/O Device," National Instruments, Austin, TX, USA), which was linked to MATLAB (MATLAB, version R2022b, The MathWorks, Inc., Natick, MA, USA) and digitized at 150 Hz. The ergometer functioned in its dynamic arrangement, and every recording was conducted under an identical wheel resistance setting (i.e., 5 on the RP3 wheel).

Each rower's own sculling shell was kitted with a PowerLine setup (version 4.12.0.0). This package comprises force sensors fixed at the foot stretcher and oarlock gates, and oar angle sensors embedded at the oarlock gates **(Figure 1)**. These sensing elements were

linked to a data-logging module located forward of the rower, which simultaneously collected data streams from an onboard GPS unit and an IMU and delivered live summary metrics, such as stroke rate and power output. PowerLine recordings were logged at 50 Hz on the module and offloaded after the rower's session ended. Furthermore, four IMUs (version 2022.0, iSen, STT Systems, San Sebastian, Spain) collecting measurements at 100 Hz were introduced: three secured along the rower's dorsal surface (pelvis, lumbar, and thoracic spine) [42] and one affixed to the hull to enable temporal alignment with the PowerLine records. These IMUs are pocket-sized and lightweight (46 g, 56 mm × 38 mm × 18 mm), minimizing interference with rowing mechanics. They house internal sensor-fusion routines that enable the direct streaming of the unit's 3D spatial attitude and free acceleration. IMU data was wirelessly transmitted to a receiver on a chase boat shadowing the athletes. Owing to this logistical limitation, iSen recordings were confined to sequences of roughly 15 successive strokes, making them considerably shorter than the traces recorded on the PowerLine logger.

Data analysis

Signals from the iSen and PowerLine setups were temporally aligned by matching the boat velocity logged through the PowerLine GPS with the boat velocity reconstructed from the acceleration output of the boat-mounted iSen IMU. In practice, the IMU acceleration sensed along the direction of travel was integrated over time and high-pass filtered (0.1 Hz) to counteract drift; the GPS-derived velocity underwent a similar filtering treatment. The timepoints corresponding to velocity minima were automatically extracted and used both to partition the rowing cycles and to deduce the instantaneous stroke rate. These steps allowed the cycles logged in the short iSen captures to be pinpointed within the much more extensive PowerLine records. Once synchronized, all on-water rowing signals were resampled at a common 100 Hz. Individual rowing cycles were demarcated relying on the starboard oar angle for scull rowing and the handle position for ergometer rowing. In each context, the lowest displacement defined the catch, and the highest displacement defined the finish. After discarding cycles contaminated by data gaps or signal artifacts, the assembled collection totaled 396 cycles for boat rowing and 2005 for ergometer rowing.

Across both modalities, our analysis was restricted to the force component acting along the principal axis of motion (set by the boat centerline and the ergometer rail). This amounts to the horizontal fraction of the foot stretcher force. Correspondingly, of the force registered at the oarlock gates, only the propulsive portion oriented along the travel direction was retained. The strain gauge fitted to the ergometer handle, by design, sensed force exclusively in one direction: chain tension.

The cable-type position transducers installed on the ergometer recorded the displacements of the handle, chest, and seat in the ergometer coordinate frame (denoted $X_{ergo}{}^{h}$, $X_{ergo}{}^{c}$, and $X_{ergo}{}^{s}$, respectively). Arm length ($X_{ergo}{}^{a}$) and trunk opening angle surrogate ($X_{ergo}{}^{t}$) were subsequently computed as:

$$X\_\{ergo\}\^\{a\} = X\_\{ergo\}\^\{h\} - X\_\{ergo\}\^\{c\} \quad (1)$$

$$X\_\{ergo\}\^\{t\} = X\_\{ergo\}\^\{c\} - X\_\{ergo\}\^\{s\} \quad (2)$$

Leg extension was taken to be identical to $X_{ergo}{}^{s}$. The velocities of the handle and of the three body segments—$V_{ergo}{}^{h}$, $V_{ergo}{}^{a}$, $V_{ergo}{}^{t}$, and $V_{ergo}{}^{l}$ —were acquired through numerical differentiation of Xerg $X_{ergo}{}^{h}$, $X_{ergo}{}^{a}$, $X_{ergo}{}^{t}$, and $X_{ergo}{}^{s}$, respectively **(Figure 2)**.

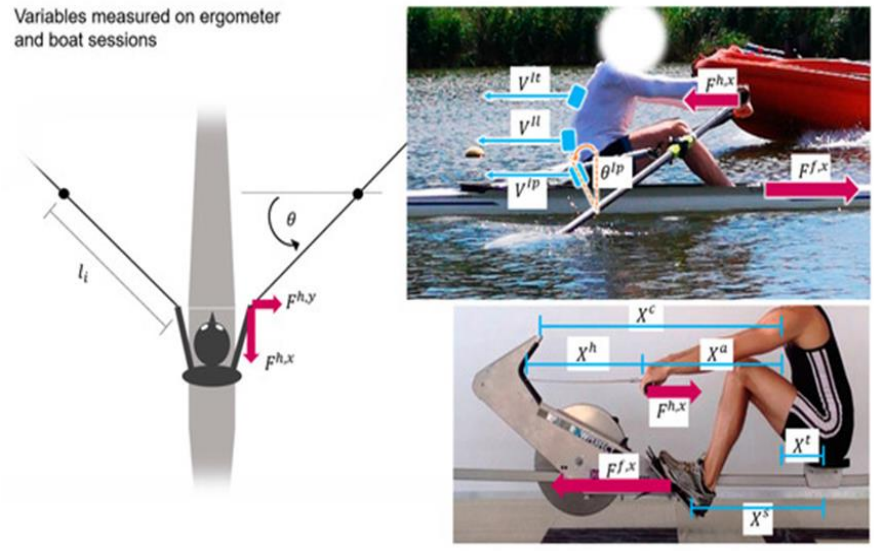

Figure 2. Graphical representation of the base variables included in the study.

For the ergometer, handle power and segmental powers were determined following the formulations of Kleshnev [44]. Concretely:

p_{ergo}^{h, x} = V_{ergo}^{h} F_{ergo}^{h, x} (3)
p_{ergo}^{a} = V_{ergo}^{a} F_{ergo}^{r h, x} (4)
p_{ergo}^{t} = V_{ergo}^{t} F_{ergo}^{h, x} (5)
p_{ergo}^{l} = V_{ergo}^{l} F_{ergo}^{r l, x} (6)

In which $P_{ergo}^{h,x}$, P_{ergo}^{a}, P_{ergo}^{t}, and P_{ergo}^{l} stand for the powers contributed by the handle, arms, trunk, and legs, respectively; $F_{ergo}^{h,x}$ is the handle force measurement; and $F_{ergo}^{f,x}$ is the horizontally resolved force measurement at the feet.

For the boat-based scenario, the corresponding powers were evaluated. However, because the instrumentation and transducers differed, a separate computational strategy was employed. Notably, the gross power imparted to the oars (P_{boat}^{h}) was calculated as:

$$P_{boat}^{h} = (F_{boat}^{h,x} l_i \cos(\theta) + F_{boat}^{h,y} l_i \sin(\theta))\dot{\theta} = P_{boat}^{h,x} + P_{boat}^{h,y}, \quad (7)$$

Where li denotes the oar's internal lever arm; $F_{boat}^{h,x}$ and $F_{boat}^{h,y}$ are the handle force components resolved along the x- and y-axes; and θ together with $\dot{\theta}$ signify the oar angle and its first time-derivative, respectively. The handle-level forces and powers represent the combined output of the port and starboard blades.

Trunk and leg segment powers were obtained as:

$$P_{boat}^{l} = P_{boat}^{f,x} V_{boat}^{l}, \quad (8)$$

$$P_{boat}^{t} = F_{boat}^{h,x} V_{boat}^{t}, \quad (9)$$

Where V_{boat}^{t} and V_{boat}^{l} are the velocities of the trunk and leg segments:

$$V_{boat}^{t} = V_{boat}^{lt} V_{boat}^{lp}, \quad (10)$$

$$V_{boat}^{l} = V_{boat}^{lp} - l^{lp} \dot{\theta}^{lp} \cos(\theta^{lp}), \quad (11)$$

In which V_{boat}^{lt} and V_{boat}^{lp} correspond to the velocities of the IMU units affixed over the thoracic spine and the pelvis, yielded by time-integration of the respective IMU acceleration streams; l^{lp} represents the separation from the pelvis IMU location to the seat (a uniform value of 15 cm was assigned for all individuals); and θ^{lp} alongside $\dot{\theta}^{lp}$ denote the tilt of the pelvis IMU relative to the vertical and its angular velocity.

The computation of arm power rested on the work of Hofmijster *et al*. [45], who posited that a rower's total mechanical power output should be equated to the power fed into the oar, summed with the power required to boost the body center of mass's velocity. Approximating the rower's body as possessing just three power-generating segments, the arm power emerges as:

$$P_{boat}^{a} = P_{boat}^{h} + \left(F_{boat}^{f,x} - F_{boat}^{h,x}\right) V_{boat} - P_{boat}^{t} - P_{boat}^{l}, \quad (12)$$

Where V_{boat} represents the boat velocity supplied by the GPS receiver built into the PowerLine unit.

In brief, the time series adopted as the target outputs for the LSTM network, subsequently labeled as 'measured sequences,' consisted of: $F^{f,x}$, $F^{h,x}$, $P^{h,x}$, P^{a}, P^{t}, P^{l}, for both ergometer and on-water rowing conditions.

LSTM architecture

A standard vanilla LSTM [40] was adopted for this work and implemented using MATLAB's Deep Learning Toolbox. Initial tests showed that adding additional LSTM layers did not meaningfully improve accuracy but did increase training time. For that reason, the random exploration was restricted to a single LSTM layer. The core network blueprint consisted of:

- Sequence input layer (nI)
- Fully connected layer (nI)
- LSTM layer
- Dropout layer (DOp)
- Fully connected layer (nO)
- Regression layer

Where nI stands for the dimensionality of the input features (18 for the on-water condition and 16 for the indoor condition) **(Table 1)**; DOp corresponds to the dropout probability; and nO denotes the count of output sequences (six for both boat and ergometer). A random search was performed to identify the optimal hyperparameter settings for the following hyperparameters: the unit count in the LSTM layer (sampled from a log-uniform distribution between 10 and 500) and the dropout probability (0%, 5%, and 10%). To select the top-performing configuration after the random exploration, the decision was guided by the mean absolute error (MAE) evaluated strictly over the effective drive portion (see the section covering LSTM performance evaluation).

Table 1. List of features included in the LSTM network for boat and ergometer cases.

Model input variables	Ergometer setup	On-water (boat) setup
Angular velocity of the oar	−	+
Horizontal velocity of the boat	−	+

Boat acceleration	−	+
Thoracic IMU horizontal velocity relative to the boat	−	+
Lumbar IMU horizontal velocity relative to the boat	−	+
Pelvic IMU horizontal velocity relative to the boat	−	+
Thoracic IMU first principal component (PCA1) acceleration	−	+
Lumbar IMU first principal component (PCA1) acceleration	−	+
Pelvic IMU first principal component (PCA1) acceleration	−	+
Thoracic IMU first principal component (PCA1) angular velocity	−	+
Lumbar IMU first principal component (PCA1) angular velocity	−	+
Pelvic IMU first principal component (PCA1) angular velocity	−	+
Mean boat velocity during the preceding stroke cycle	−	+
Peak boat velocity in the preceding stroke cycle	−	+
Athlete height	+	+
Athlete's body mass	+	+
Duration of the previous drive phase	+	+
Duration of the current drive phase	+	+
Handle position	+	−
Chest position	+	−
Seat position	+	−
Handle velocity	+	−
Arm velocity	+	−
Trunk velocity	+	−
Seat velocity	+	−
Handle acceleration	+	−
Trunk acceleration	+	−
Leg acceleration	+	−
Maximum handle velocity in the previous stroke cycle	+	−
Time interval from peak handle velocity to the start of the current cycle	+	−

[1] First principal component.

LSTM training

Training was first performed during the random search phase, after which the identified architecture was used in a leave-one-out validation procedure (similar to the protocol described by Su *et al*. [36]). During random search training, the available data were split into 80% for training and 20% for validation. For leave-one-out validation, N–1 subjects formed the training pool, and the single excluded subject served as the validation case, with the procedure repeated N times. An early-stopping rule halted training after 20 epochs [46] without a reduction in the reconstruction discrepancy on the validation split, quantified as the root mean squared error (RMSE) over a complete rowing cycle [36]. The training parameters were assigned as follows: maximum epochs: 10,000; learning rate: 0.001; mini-batch size: 32; Adam optimizer. Separate LSTM models were fitted for the ergometer and boat sessions.

LSTM data

Across both the ergometer and boat scenarios, the target outputs covered six time series: Ff,x, Fh,x, Ph,x, Pa, Pt, and Pl. In each setting, these sequences were cut into rowing cycles spanning from one finish event to the next. The cycles were preserved in their original absolute time rather than being normalized in duration. Before training, all variables were centered and scaled by their means and standard deviations. The set of input features differed between the ergometer and the boat owing to distinct sensing modalities and the fact that the two environments involve different body mechanics and external interactions. For the ergometer LSTM, 16 features were supplied: positions of the handle, chest, and seat (Xh, Xc, and Xs); velocities of the handle, arms, trunk opening, and leg extension (Vh, Va, Vt, and Vl); plus trunk and leg accelerations computed as the time derivatives of the matching velocity signals. Several additional features encoded subject anthropometrics and session descriptors: rower height and weight, the lengths of the preceding and current drive periods, the maximal handle speed attained in the prior stroke, and the delay separating that speed peak from the catch of the ongoing stroke. The reasoning behind the last two features is that handle resistance is governed by the flywheel's rotational rate, which decays during recovery when no drive force acts on it. Consequently, the elapsed interval since the speed maximum should reflect the flywheel's spinning rate at drive onset. For the boat LSTM, 18 features were provided: gate angular velocity ($\theta^{\cdot}$); boat horizontal velocity (derived from the GPS inside the PowerLine box) and acceleration (from the

accelerometer housed in the same box); horizontal velocities of the thoracic, lumbar, and pelvis IMUs expressed in the boat coordinate frame (VboatIt, VboatIl, and VboatIp); and the first principal component extracted from the acceleration and angular velocity signals of the three IMUs. In parallel with the ergometer strategy, extra features conveyed subject-level and session-level data: rower height and weight; mean and maximal boat velocities registered over the preceding cycle (which contain indirect information on boat speed alterations and, hence, on the energy imparted to the oars); and the lengths of the prior and present drive periods (which offer cues about the stroke rate, a variable recognized to correlate with power output).

LSTM performance evaluation

Network performance was compared using metrics restricted to the effective drive phase, since forces and powers remain negligible throughout recovery and offer little value for evaluation. The boundaries of the effective drive phase, in both ergometer and boat trials, were automatically detected within each cycle by applying the same logic used in the Peach software: the phase began when the gate force exceeded 20 kg and ended when it fell below 10 kg. Although ergometer trials at multiple stroke rates contributed to LSTM training to promote broader generalizability of the reconstructions, the downstream performance analyses drew exclusively from the 20 spm sessions, which provided the greatest number of consistent, artifact-free cycles. Two error metrics were employed: the mean absolute error (MAE) evaluated across all cycles between the reference and reconstructed sequences (i.e., Ff,x, Fh,x, Ph,x, Pa, Pt, Pl), and the MAE computed on the mean curve obtained by averaging across cycles (cMAE). Because cycle durations varied, each reconstructed sequence was resampled onto a fixed grid of 50 time points delineating the effective drive phase.

$$MAE = \frac{1}{CT}\sum_{c=1}^{C}\sum_{t=1}^{T}\left|y_t^c - \widehat{y}_t^c\right|, \tag{13}$$

$$cMAE = \frac{1}{CT}\sum_{t=1}^{T}\left|\sum_{c=1}^{C}\left(y_t^c - \widehat{y}_t^c\right)\right|, \tag{14}$$

Where T = 50 time points; C equals the number of cycles present in the validation fold. For leave-one-out validation, C corresponds to the totality of cycles linked to a single individual. Both MAE and cMAE were additionally conveyed as proportions of the signal magnitude:

$$(c)MAE_{norm} = \frac{(c)MAE}{mean(|V|)}, \tag{15}$$

Where V denotes any of the time-normalized target quantities.

We further probed how the estimation procedure affected technical determinants habitually employed to characterize and assess rowing technique. These consisted of the time to peak (T2P), denoting the instant the curve reaches its maximum, quoted as a percentage of the complete drive phase (catch to finish); the mean to peak ratio (M2P), which is the ratio of the mean value to the peak value over the drive phase, multiplied by 100; and the work ratio (WR), representing the fraction of the area under the curve lying before the peak divided by the entire area under the curve, again multiplied by 100 and evaluated across the full drive phase [17]. To ascertain whether rower technique could be faithfully represented by the estimated sequences, we applied two-sample t-tests (MATLAB ttest2 function, $\alpha = 0.05$) to contrast the mean technical determinant scores obtained from the measured data with those derived from the LSTM-estimated sequences. We likewise verified whether the estimated technical determinants retained the ability to distinguish between the techniques of distinct athletes—specifically, in situations where the measured technical scores of two individuals already showed statistically significant separation. This involved running two-sample t-tests between every possible rower pair. Owing to insufficient per-subject cycle counts in certain boat-session cases, inter- and intrasubject t-tests were applied exclusively to the ergometer dataset.

For intrasubject comparisons, accuracy was formulated as:

$$As = \frac{HA}{HA + HR} * 100, \tag{15}$$

With HA representing the count of subjects for whom the null hypothesis of equal means could not be discarded (P-value > 0.05), and HR the count of subjects for whom that null hypothesis was discarded.

For inter-subject comparisons, accuracy was formulated as:

$$Ap = \frac{CH}{CH + DH} * 100, \tag{16}$$

In which CH counts subject pairs where the decision regarding the null hypothesis (that the two subjects share equal means for the technical determinant under scrutiny) was identical—whether rejected or retained—for both the measured and LSTM-based curves; DH tallies the subject pairs for which the null hypothesis decision was inconsistent between the measured and estimated data.

Results and Discussion

The hyperparameter search settled on 1 layer, 500 neurons, and 0% dropout as the optimal configuration for the

ergometer case, and 1 layer, 53 neurons, with 10% dropout for the boat case. The grand-average measured and estimated force and power curves for four representative participants in the ergometer and boat datasets are plotted in **Figure 3**. **Table 2** summarizes, across all subjects, the absolute and normalized MAE and cMAE values obtained for each force and power variable. The pooled MAEnorm means were 3.20% and 4.90% for ergometer and boat sessions, respectively; the pooled cMAEnorm means were 0.53% and 0.90% for ergometer and boat sessions, respectively. Under leave-one-out validation, the MAEnorm averaged 19.94% and 14.02% for the ergometer and boat conditions, respectively **(Table 2)**; the corresponding cMAEnorm means were 7.95% and 12.38%. **Figure 4** displays the same performance indices broken down per participant. The variable yielding the highest MAE and cMAE was Ph, whereas the variable recording the largest MAEnorm and cMAEnorm was Pa.

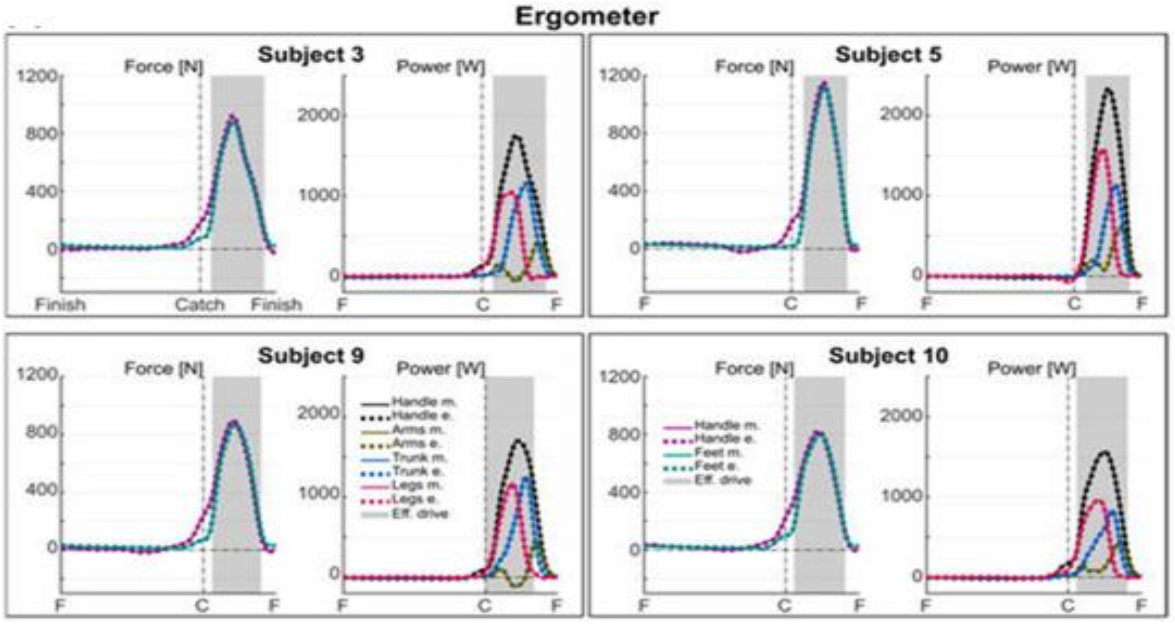

a)

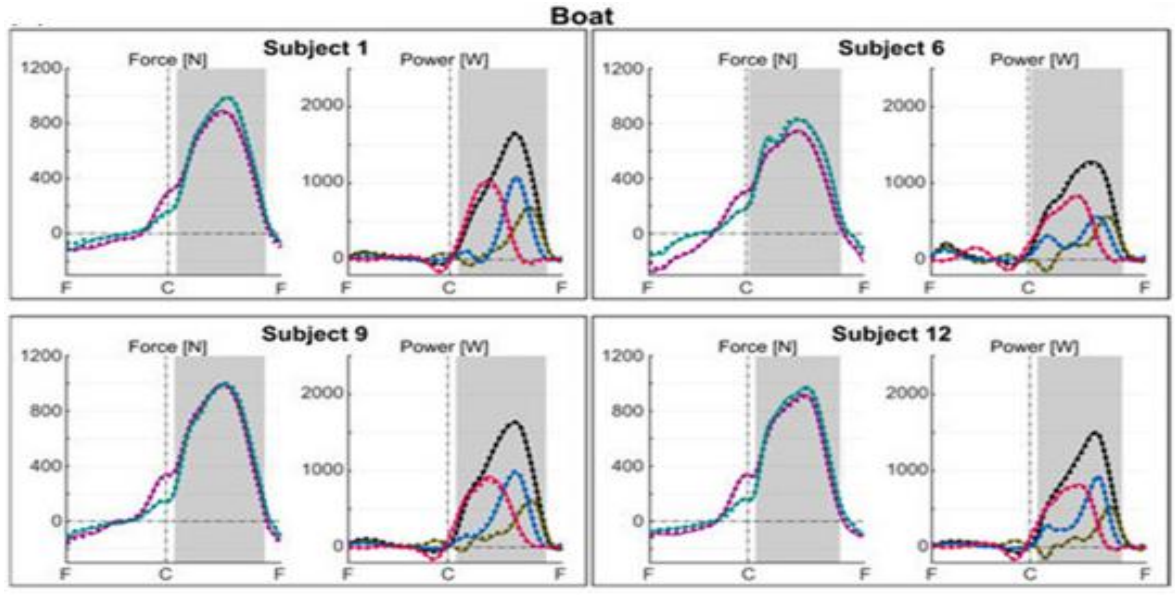

b)

Figure 3. Reference (solid traces) and reconstructed (dashed traces) force and power waveforms for four illustrative participants during ergometer (a) and on-water (b) rowing. Each trace corresponds to the mean computed across all validation cycles, temporally normalized to the finish-to-finish interval. The catch instant is marked by the vertical rule; the shaded band highlights the effective drive phase.

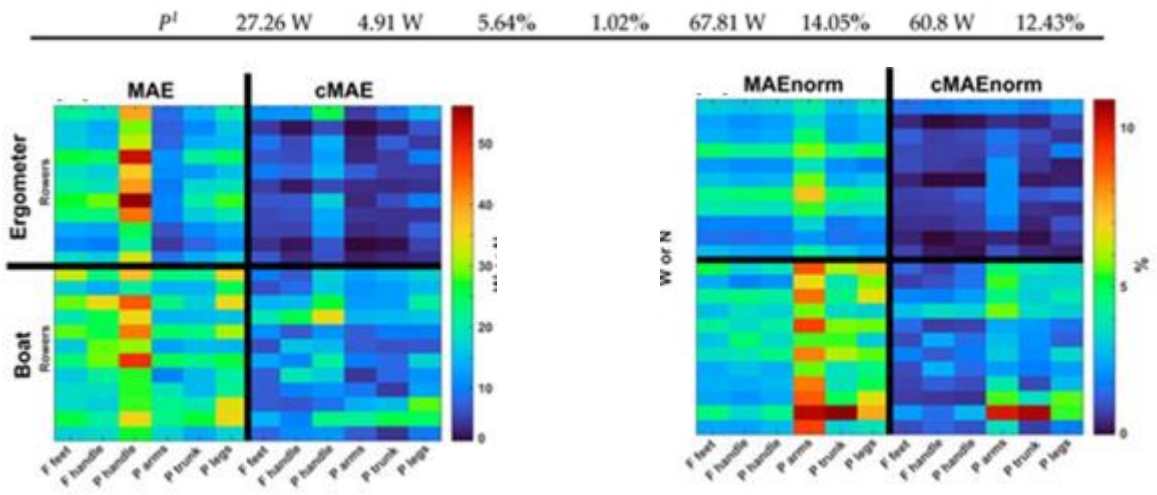

a) b)

Figure 4. The MAE and cMAE values are displayed both in their raw, absolute magnitudes (a) and after normalization by the mean amplitude of the corresponding target curve (b). Forces (F) are expressed in N, while powers (P) are expressed in W. Each row of the figure corresponds to a single rower.

Table 2. LSTM performance summary. Absolute and normalized MAE and cMAE figures are reported for the cycles comprising the validation set. The leave-one-out validation (LOOV) results represent the mean errors averaged across all subjects.

Condition	Variable	LOOV normalized cMAE	LOOV cMAE	LOOV normalized MAE	LOOV MAE	Normalized cMAE	Normalized MAE	cMAE	MAE
Ergometer	Ff,x	9.22%	58.74 N	10.40%	66.20 N	0.43%	3.06%	2.67 N	19.15 N
	Fh,x	6.32%	39.53 N	7.63%	47.73 N	0.39%	2.87%	2.40 N	17.69 N
	Ph,x	6.30%	78.55 W	7.69%	95.81 W	0.43%	2.96%	5.44 W	37.04 W
	Pa	11.23%	22.37 W	13.24%	26.26 W	0.88%	4.40%	1.77 W	8.87 W
	Pt	5.55%	28.43 W	7.05%	35.64 W	0.33%	2.88%	1.68 W	14.50 W
	Pl	9.07%	57.79 W	10.20%	59.43 W	0.71%	3.05%	4.20 W	18.07 W
Boat	Ff,x	10.49%	65.94 N	11.54%	72.80 N	0.57%	3.58%	3.66 N	22.89 N
	Fh,x	7.67%	52.71 N	8.91%	61.40 N	0.59%	3.33%	4.13 N	23.15 N
	Ph,x	10.03%	97.48 W	11.29%	110.17 W	0.52%	3.55%	5.14 W	34.76 W
	Pa	22.39%	53.43 W	25.15%	60.89 W	1.26%	8.25%	3.13 W	20.52 W
	Pt	11.25%	39.48 W	13.19%	46.89 W	1.43%	5.06%	5.38 W	19.01 W
	Pl	12.43%	60.8 W	14.05%	67.81 W	1.02%	5.64%	4.91 W	27.26 W

The technique-defining metrics that characterize a rower's stroke (i.e., T2P, M2P, and WR) are presented in **Figure 5** for four illustrative athletes. A well-defined proximal-to-distal coordination pattern—legs, followed by trunk, then arms—was evident in both on-water and ergometer rowing, with T2P situated near 40%, 60%, and 70% of the cycle, respectively. Athletes tested on the ergometer adopted noticeably different approaches to arm recruitment, as demonstrated by the between-subject dispersion in M2P and WR. Among those tested on the water, trunk and leg involvement patterns showed more pronounced variation from one individual to another. The aggregate MAE values for T2P were 0.78% and 1.55%; for M2P, 0.66% and 0.96%; and for WR, 2.05% and 3.32%, reported for boat and ergometer trials, respectively **(Table 3)**. When restricting the lens to ergometer data, no statistically reliable offsets were detected when comparing T2P, M2P, and WR figures extracted from LSTM-predicted traces with those derived from directly instrumented recordings **(Figure 6)**. In head-to-head comparisons across subjects, the capacity to distinguish one rower from another using T2P calculated from arm, trunk, and leg power traces yielded accuracy scores of 90.9%, 94.5%, and 90.9%, respectively. The corresponding accuracy rates climbed to 94.5%, 96.4%, and 98.2% when relying on M2P, and registered at 98.2%, 85.4%, and 90.9% when classification rested on the WR of each segment.

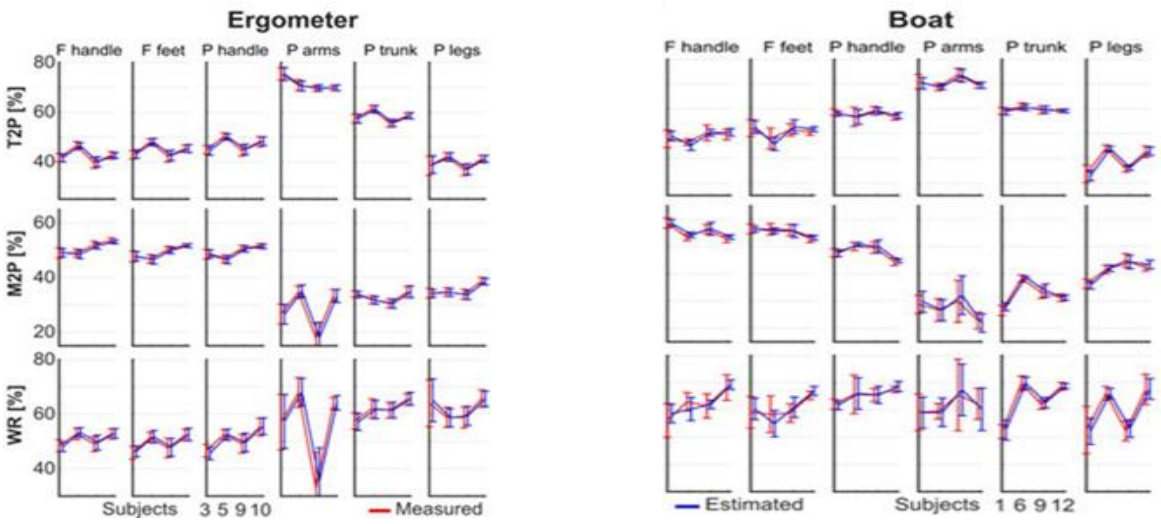

Figure 5. The technical metrics T2P, M2P, and WR, evaluated on the directly recorded (red) and LSTM-predicted (blue) force and power waveforms, are shown for four representative participants from the ergometer (a) and on-water (b) trials. Each bar represents the mean and standard deviation aggregated across all cycles in the validation set.

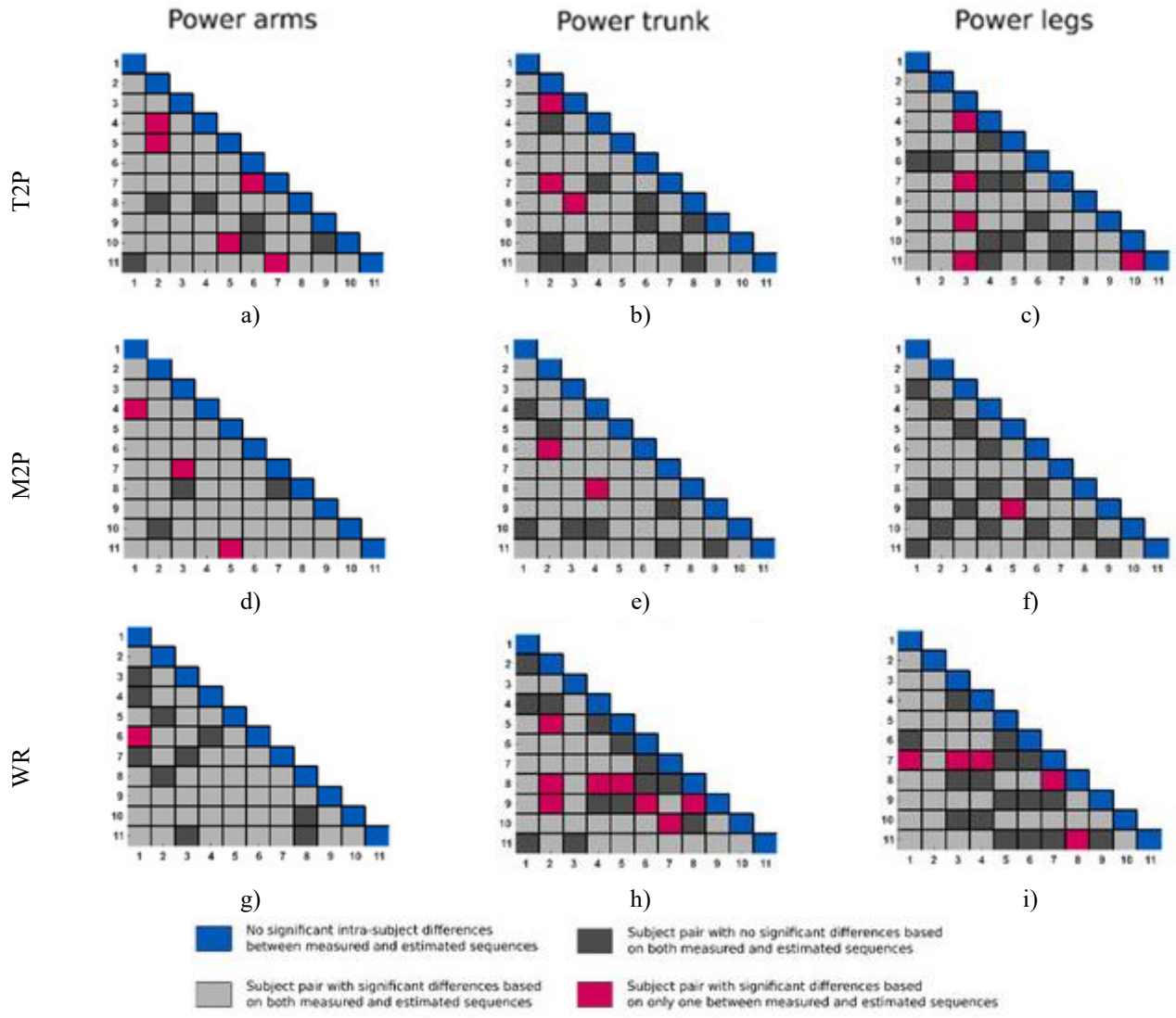

Figure 6. Depiction of two-sample t-test comparisons between the directly instrumented and LSTM-inferred traces for the T2P, M2P, and WR metrics derived from the power contributions of the arms, trunk, and legs. Cells along the main diagonal

capture how a single subject's measured and predicted profiles compare. Cells away from the diagonal reflect head-to-head tests between different subjects, each conducted separately on the experimentally recorded data and on the network-generated estimates. The shading denotes whether a between-subject distinction uncovered in the estimated outputs matches the distinction observed in the measured data.

Table 3. Grand mean ± standard deviation alongside the mean absolute error (MAE) tallied over every cycle belonging to the validation partition, reported for the technical metrics time to peak (T2P), mean to peak ratio (M2P), and work ratio (WR).

Condition	Variable	WR error (MAE)	Work ratio (%)	M2P error (MAE)	Magnitude to peak (%)	T2P error (MAE)	Time to peak (% drive phase)
Ergometer	Ff,x	2.07	0.11 ± 2.93	0.86	−0.25 ± 1.09	0.97	0.05 ± 1.59
	Fh,x	2.18	−0.08 ± 3.01	0.75	−0.16 ± 1.03	1.06	0.02 ± 1.69
	Ph,x	2.04	−0.15 ± 2.92	0.80	−0.13 ± 1.06	0.96	0.00 ± 1.61
	Pa	2.25	0.33 ± 3.55	0.59	0.04 ± 0.78	0.48	−0.07 ± 1.07
	Pt	1.51	−0.12 ± 3.45	0.47	−0.05 ± 0.63	0.42	−0.02 ± 1.44
	Pl	2.25	0.15 ± 4.30	0.48	−0.12 ± 0.65	0.80	0.23 ± 1.92
Boat	Ff,x	4.88	0.59 ± 6.15	1.15	0.17 ± 1.39	2.67	0.31 ± 3.45
	Fh,x	4.13	0.49 ± 5.99	0.89	−0.16 ± 1.11	2.39	0.20 ± 3.49
	Ph,x	2.35	0.48 ± 3.12	0.74	0.25 ± 0.92	1.22	0.11 ± 1.72
	Pa	3.15	−0.28 ± 4.17	1.26	0.44 ± 1.64	0.88	−0.34 ± 1.17
	Pt	1.89	0.29 ± 2.37	0.80	0.55 ± 0.92	0.57	−0.06 ± 0.83
	Pl	3.55	0.84 ± 4.92	0.96	−0.19 ± 1.28	1.54	0.26 ± 2.27

This paper proposes an approach to infer the forces and powers generated during rowing that requires minimal equipment setup and entirely avoids mounting force transducers. The intent was to devise a straightforward tool that coaches could integrate into routine training and that might eventually underpin live feedback for athletes. By comparison, resorting to classical biomechanical modeling frameworks [31, 33] would entail considerably more elaborate simulations, requiring skilled operators and longer processing pipelines. Owing to the inherently sequential nature of rowing and the direct velocity–power relationship it entails, we selected an LSTM architecture, given its established track record of delivering robust outcomes on sequential motor tasks such as walking [36]. The LSTM network demonstrated the ability to reconstruct rower-generated forces and powers, with a pooled mean absolute error below 5% in both ergometer and on-water conditions. Averaging over multiple consecutive cycles—a step warranted by the rhythmic and highly stereotyped character of the rowing action [47]—further compressed the mean error to below 1%. Moreover, each rower's individual technical signature, parameterized by peak timing, mean-to-peak ratio, and work ratio, was recovered by the LSTM with an error smaller than 4%. Lastly, inter-individual contrasts in rowing style were detected with an accuracy exceeding 90%, except for the trunk power work ratio during ergometer rowing. The method put forward, therefore quantified, with fair precision, quantities that matter for gauging both rowing output [1, 13] and technical execution [9, 12, 17].

The fidelity of the reconstructed traces was sufficient to pick up subtle features of a rower's technique that could be targeted during coaching. To illustrate, in **Figure 3a**, the ergometer rowers exhibit distinct patterns of arm power generation: subject 9 shows an early peak, immediately followed by a period of negative power. A profile of this type is regarded as a technical deficiency [1, 48] because it implies that a portion of the power the rower generates is being absorbed by the arms rather than being transmitted onward to the handle or oars. For this specific athlete, the proposed pipeline would make it possible to deliver focused feedback aimed at remedying the detected flaw (e.g., reducing the negative power, displayed on a screen placed ahead of the rower) while simultaneously yielding objective indicators the coach can monitor longitudinally (e.g., the wattage of negative power, ideally trending toward zero). Live augmented feedback has already demonstrated its utility in both on-water and ergometer contexts [11, 48, 49], and the prospect of supplying targeted feedback with minimal instrumentation across both settings would offer considerable advantages to practitioners and rowers alike.

Body segment power estimates were less precise than force estimates, particularly for arm power, which contributed the least and showed the largest relative discrepancy. This outcome was anticipated, since forces are directly sensed quantities, whereas segmental power computations rest on a chain of assumptions that combine multiple measurement streams. For example, variation in sensor placement across participants can lead to over- or underestimation of arm length and arm velocity,

introducing noise into the power derivation without affecting the force recordings. Additional noise sources that cap the LSTM's performance were also identified. First, the forces collected were uniaxial, yet in practice rowers also generate vertically and laterally directed forces that influence boat and ergometer behavior and are not registered by the sensors. Other noise contributors, while they degrade the network's cycle-to-cycle accuracy, can be attenuated by averaging over several strokes. These contributors notably include environmental interactions with water and wind, which can fluctuate within a single outing [50], as well as oscillations of the ergometer along its rail. For instance, while the mean displacement of the ergometer over many cycles is clearly zero, individual cycles may see the system's center of mass (rower plus machine) migrate a few centimeters forward or backward. These run-to-run variations mean the model, at its present stage, is not yet suited for pinpointing instantaneous shifts in an athlete's technique. Still, given the strong consistency of the rowing movement [47], data collapsed over a modest number of cycles will yield meaningful insights into technical development and performance evolution over time. Certain quantities may be more susceptible to these inaccuracies than others, such as the T2P of a waveform featuring a broad plateau, where minor perturbations can have an outsized effect on the detected peak location (e.g., for ergometer subject 3, leg power T2P proved less reliable for distinguishing between athletes). While the current method may fall short of discriminating between rowers whose techniques are extremely alike, the errors in recovering technical determinants were smaller than the natural spread observed across individuals employing distinctly different styles. Indeed, the technical metrics used to profile rowers' stroke execution exhibited strong correspondence between the directly instrumented and the LSTM-predicted traces. When contrasting the techniques of pairs of rowers, the determinants derived from the reconstructed outputs achieved 93% accuracy, indicating that the legs–trunk–arms coordination sequence could be faithfully estimated and applied to guide crew selection based on the similarity of force and power profiles [16].

The force and power reconstruction fidelity dropped considerably under leave-one-out validation, and the degree of degradation varied widely across participants. Such an outcome was anticipated given the modest cohort size. The rowers enrolled in the study spanned a broad spectrum in terms of stature, body mass, and stroke mechanics, and individual cases could easily fall beyond the distribution represented by a small training pool. Future efforts should gather a substantially larger dataset to bolster generalizability across more diverse rowing populations [1]. Notably, the present sample was limited to male athletes of comparable age, proficiency tier, and technical style [1]. Broadening data collection to include female rowers and individuals from younger and older age brackets is an essential step toward incorporating a wider range of body types into the training corpus.

Furthermore, augmenting the dataset with measurements from less experienced rowers (e.g., novices or recreational gym users) may help the model capture the underlying mechanics of the rowing stroke that would otherwise be underrepresented when relying exclusively on data from highly skilled performers. Incorporating these additional data streams could pave the way for a computational pipeline capable of predicting forces, powers, and technical signatures for any rower, irrespective of the rowing modality. That said, even in its current form—with a network trained on a limited dataset roughly matching the size of a typical rowing club—the approach yields encouraging outcomes, enabling the reconstruction of individual technical patterns across different settings, as long as the athlete has undergone a single prior assessment with the complete sensor suite. Building on these encouraging findings, future studies should investigate the feasibility of inferring force and power solely from video footage. Such video-driven techniques have already been successfully deployed for more complex motor tasks [25], and their translation to rowing, particularly within the predictable setting of an indoor ergometer, appears entirely feasible.

Taken together, the presented methodology stands to markedly lower the financial burden of performance diagnostics. Outfitting an ergometer with nothing more than cable-based position sensors could slash costs by over half, and video-based alternatives could yield even more dramatic savings. Along similar lines, while the expense of instrumenting a boat currently surpasses EUR 2000, a collection of IMUs and GPS modules can be sourced for under half that amount, with the added benefit of being readily transferable across different athletes and hulls.

In summary, fitting rowing shells and ergometers with force and displacement instrumentation is expensive and labor-intensive. The method introduced here requires only the placement of IMUs or cable sensors (and, ideally, for indoor settings, these could eventually be supplanted by video-based motion capture). It can accurately assess both the output and the technical execution of rowers.

Conclusion

This study highlights the growing issue of fluoroquinolone resistance in E. coli strains, particularly in UTIs. In-silico docking revealed that novel derivatives, such as SP9, SP12, SP25, and SP42, exhibited stronger binding to bacterial DNA gyrase compared to traditional fluoroquinolones, showing potential as next-generation treatments. Further optimisation is necessary, nevertheless, due to worries about mutagenicity and other

toxicities in SP9, SP12, and SP25. Conversely, 2-4 Difluoro Benzene with morpholino scaffolds [SP42] was a perfect candidate for continued development because it passed all analyses, including the toxicity prediction. In order to successfully address resistance mechanisms, future research should concentrate on in-vitro and in-vivo evaluations and investigate combination therapy.

Acknowledgments: The authors would like to thank the trainers and athletes of the Pôle Aviron Nancy for their availability and valuable support.

Conflict of interest: None

Financial support: This research was funded by a grant from the PIA (Programme d'Investissements d'Avenir) via the ANR (Agence Nationale de la Recherche) with the reference ANR-20-STHP-0006.

Ethics statement: This study was approved by the Sud-Ouest et Outre-Mer III ethics committee (approval reference 20.07.21.43000-ID_9115) and complied with the requirements of the Declaration of Helsinki.
Written informed consent was obtained from all subjects involved in the study.

References

1. Kleshnev V. The biomechanics of rowing. 2nd ed. Marlborough, UK: Crowood Press; 2016.
2. Dawson RG, Lockwood RJ, Wilson JD, Freeman G. The rowing cycle: sources of variance and invariance in ergometer and on-the-water performance. J Mot Behav. 1998;30(1):33–43.
3. Colloud F, Bahuaud P, Doriot N, Champely S, Chèze L. Fixed versus free-floating stretcher mechanism in rowing ergometers: mechanical aspects. J Sports Sci. 2006;24(5):479–93.
4. Mpimis T, Gikas V, Gourgoulis V. A rigorous and integrated on-water monitoring system for performance and technique improvement in rowing. Sensors. 2023;23:6150.
5. Warmenhoven J, Cobley S, Draper C, Harrison AJ, Bargary N, Smith R. Assessment of propulsive pin force and oar angle time-series using functional data analysis in on-water rowing. Scand J Med Sci Sports. 2017;27(10):1688–96.
6. Warmenhoven J, Cobley S, Draper C, Harrison A, Bargary N, Smith R. How gender and boat-side affect shape characteristics of force–angle profiles in single sculling: insights from functional data analysis. J Sci Med Sport. 2018;21(6):533–7.
7. Warmenhoven J, Cobley S, Draper C, Smith R. Over 50 years of researching force profiles in rowing: what do we know? Sports Med. 2018;48(11):2703–14.
8. Holt AC, Ball K, Siegel R, Hopkins WG, Aughey RJ. Relationships between measures of boat acceleration and performance in rowing, with and without controlling for stroke rate and power output. PLoS One. 2021;16:e0249122.
9. Holt AC, Aughey RJ, Ball K, Hopkins WG, Siegel R. Technical determinants of on-water rowing performance. Front Sports Act Living. 2020;2:589013.
10. Lintmeijer LL, Hofmijster MJ, Schulte Fischedick GA, Zijlstra PJ, Van Soest AJ. "Knoek" improved determination of mechanical power output in rowing: experimental results. J Sports Sci. 2018;36(20):2138–46.
11. Lintmeijer LL, Knoek Van Soest AJ, Robbers FS, Hofmijster MJ, Beek PJ. Real-time feedback on mechanical power output: facilitating crew rowers' compliance with prescribed training intensity. Int J Sports Physiol Perform. 2019;14(3):303–9.
12. Pitto L, Ertel GN, Simon FR, Gauchard GC, Mornieux G. Influence of neuromuscular activity and technical determinants on scull rowing performance. Appl Sci. 2024;14:9055.
13. Smith R, Draper C. Skill variables discriminate between the elite and sub-elite in coxless pair-oared rowing. Int Soc Biomech Sport. 2006;24:1–4.
14. Trompeter K, Fett D, Platen P. Back pain in rowers: a cross-sectional study on prevalence, pain characteristics and risk factors. Sportverletz Sportschaden. 2019;33(1):51–9.
15. Wilson F, Thornton JS, Wilkie K, Hartvigsen J, Vinther A, Ackerman KE, et al. 2021 consensus statement for preventing and managing low back pain in elite and subelite adult rowers. Br J Sports Med. 2021;55(13):893–9.
16. Baudouin A. A biomechanical review of factors affecting rowing performance. Br J Sports Med. 2002;36(5):396–402.
17. Simon FR, Ertel GN, Duchene Y, Maciejewski H, Gauchard GC, Mornieux G. Prediction of rowing ergometer performance by technical and core stability parameters. J Sports Sci. 2023;41(4):399–407.
18. Pitto L, Simon F, Banet L, Ertel G, Mornieux G. Real-time biofeedback to control trunk power production in ergometer rowing. ISBS Proc Arch. 2024;42:760.
19. Warmenhoven J, Smith R, Draper C, Harrison AJ, Bargary N, Cobley S. Force coordination strategies in on-water single sculling: are asymmetries related to better rowing performance? Scand J Med Sci Sports. 2018;28(4):1379–88.
20. Ejaz N, Khan SJ, Azim F, Asif M, Teuțan E, Pleșa A, et al. Automatic gait classification model empowered by machine learning for people with and without

osteoporosis using smart walker. Appl Sci. 2024;14:3874.
21. Yang Z. An efficient automatic gait anomaly detection method based on semisupervised clustering. Comput Intell Neurosci. 2021;2021:8840156.
22. Worsey MTO, Pahl R, Espinosa HG, Shepherd JB, Thiel DV. Is machine learning and automatic classification of swimming data what unlocks the power of inertial measurement units in swimming? J Sports Sci. 2021;39(17):2095–114.
23. Stetter BJ, Ringhof S, Krafft FC, Sell S, Stein T. Estimation of knee joint forces in sport movements using wearable sensors and machine learning. Sensors. 2019;19:3690.
24. Matijevich ES, Scott LR, Volgyesi P, Derry KH, Zelik KE. Combining wearable sensor signals, machine learning and biomechanics to estimate tibial bone force and damage during running. Hum Mov Sci. 2020;74:102690.
25. Johnson WR, Mian A, Donnelly CJ, Lloyd D, Alderson J. Predicting athlete ground reaction forces and moments from motion capture. Med Biol Eng Comput. 2018;56(10):1781–92.
26. ForceTeck. Available from: https://www.forceteck.com/(accessed 2024 Dec 24).
27. Model Health. Available from: https://www.modelhealth.io(accessed 2024 Dec 24).
28. Wilaikaew P, Noisriphan W, Chen CC, Charoensuk J, Ruengitinun S, Chootong C. Apply machine-learning model for clustering rowing players. In: Proceedings of the ACM International Conference Proceeding Series. Osaka, Japan; 2023. pp. 218–24.
29. Bosch S, Shoaib M, Geerlings S, Buit L, Meratnia N, Havinga P. Analysis of indoor rowing motion using wearable inertial sensors. In: Proceedings of the BodyNets International Conference on Body Area Networks. Sydney, Australia; 2015.
30. Li Y, Koldenhoven R, Jiwan N, Zhan J, Liu T. Automated rower assignment to rowing events: a machine learning approach. ISBS Proc Arch. 2024;42:592.
31. Nitschke BJ, Marzilger R, Leyendecker S, Eskofier BM, Koelewijn AD. Change the direction: 3D optimal control simulation by directly tracking marker and ground reaction force data. PeerJ. 2023;11:e14852.
32. Dorschky E, Nitschke M, Seifer AK, van den Bogert AJ, Eskofier BM. Estimation of gait kinematics and kinetics from inertial sensor data using optimal control of musculoskeletal models. J Biomech. 2019;95:109278.
33. Falisse A, Pitto L, Kainz H, Hoang H, Wesseling M, Van Rossom S, et al. Physics-based predictive simulations to explore the differential effects of motor control and musculoskeletal deficits on gait dysfunction in cerebral palsy: a retrospective case study. Front Hum Neurosci. 2020;14:497821.
34. Ordóñez F, Roggen D. Deep convolutional and LSTM recurrent neural networks for multimodal wearable activity recognition. Sensors. 2016;16:115.
35. Nait Aicha A, Englebienne G, Van Schooten KS, Pijnappels M, Kröse B. Deep learning to predict falls in older adults based on daily-life trunk accelerometry. Sensors. 2018;18:1654.
36. Su B, Gutierrez-Farewik EM. Gait trajectory and gait phase prediction based on an LSTM network. Sensors. 2020;20:7127.
37. Zaroug A, Lai DTH, Mudie K, Begg R. Lower limb kinematics trajectory prediction using long short-term memory neural networks. Front Bioeng Biotechnol. 2020;8:527709.
38. Greff K, Srivastava RK, Koutník J, Steunebrink BR, Schmidhuber J. LSTM: a search space odyssey. IEEE Trans Neural Netw Learn Syst. 2016;28(9):2222–32.
39. Graves A. Generating sequences with recurrent neural networks. arXiv. 2013:arXiv:1308.0850.
40. Zaroug A, Garofolini A, Lai DTH, Mudie K, Begg R. Prediction of gait trajectories based on long short term memory neural networks. PLoS One. 2021;16:e0255597.
41. Brice SM, Millett EL, Philippa B. The validity of using inertial measurement units to monitor the torso and pelvis sagittal plane motion of elite rowers. J Sports Sci. 2022;40(9):950–8.
42. Li Y, Koldenhoven RM, Jiwan NC, Zhan J, Liu T. Trunk and shoulder kinematics of rowing displayed by Olympic athletes. Sports Biomech. 2020;22(8):1095–107.
43. Chia L, Andersen JT, McKay MJ, Sullivan J, Megalaa T, Pappas E. Evaluating the validity and reliability of inertial measurement units for determining knee and trunk kinematics during athletic landing and cutting movements. J Electromyogr Kinesiol. 2021;60:102589.
44. Kleshnev V. Power in rowing. In: Proceedings of the 18th International Symposium on Biomechanics in Sports. Hong Kong; 2000. pp. 2–5.
45. Hofmijster MJ, Lintmeijer LL, Beek PJ, van Soest AJK. Mechanical power output in rowing should not be determined from oar forces and oar motion alone. J Sports Sci. 2018;36(20):2147–53.
46. Karakish M, Fouz MA, Elsawaf A. Gait trajectory prediction on an embedded microcontroller using deep learning. Sensors. 2022;22:8441.
47. Fohanno V, Nordez A, Smith R, Colloud F. Asymmetry in elite rowers: effect of ergometer design and stroke rate. Sports Biomech. 2015;14(3):310–22.
48. Gorman AJ, Willmott AP, Mullineaux DR. The effects of concurrent biomechanical biofeedback on

novel skill acquisition. Sports Biomech. 2022;21(3):297–311.
49. Gorman AJ, Willmott AP, Mullineaux DR. The effects of concurrent biomechanical biofeedback on rowing performance at different stroke rates. J Sports Sci. 2021;39(20):2716–26.
50. Binnie MJ, Astridge D, Watts SP, Goods PSR, Rice AJ, Peeling P. Quantifying on-water performance in rowing: a perspective on current challenges and future directions. Front Sports Act Living. 2023;5:1101654.